Interference Pattern of Floquet Modes in Frequency Space

Du-Yi Ou-Yang[1,2], Yan-Hua Zhou[1,2], Ya Zhang[3], Xiao-Tong Lu[4,5], Hong Chang[4,5], Tao Wang[1,2*], and Xue-Feng Zhang[1,6*]

[1]*Department of Physics, and Chongqing Key Laboratory for Strongly Coupled Physics, Chongqing University, Chongqing 401331, China*
[2]*Center of Modern Physics, Institute for Smart City of Chongqing University in Liyang, Liyang 213300, China*
[3]*School of Instrumentation Science and Engineering, Harbin Institute of Technology, Harbin 150000, China*
[4]*Key Laboratory of Time and Frequency Primary Standards, National Time Service Center, Chinese Academy of Sciences, Xi'an 710600, China*
[5]*School of Astronomy and Space Science, University of Chinese Academy of Sciences, Beijing 100049, China*
[6]*Center of Quantum Materials and Devices, Chongqing University, Chongqing 401331, China*

(Received 1 April 2025; accepted manuscript online 21 May 2025)

Wave–particle duality is one of the key features of quantum physics, characterized by the interference pattern. Meanwhile, Floquet spectroscopy is typically studied in the high-frequency region because the Floquet sidebands are very sharp, behaving like "particles" in frequency space, and no interference phenomena are observed. Here, we consider the larger quantum fluctuation region where the Floquet sidebands are broader, making interference between them possible. With the help of an optical lattice clock experimental platform and numerical simulations, such interference of Floquet modes in frequency space is clearly observed. Additionally, it exhibits many exotic phenomena, such as large Floquet sidebands between integer ones, sensitivity to the initial phase, and corresponding emergent symmetries. To analytically elucidate this, we propose the Floquet channel interference hypothesis, which surprisingly matches quantitatively well with both experimental and numerical results. Our research paves the way for developing a new type of interferometer that could be applicable to other Floquet systems.

DOI: 10.1088/0256-307X/42/6/060601 CSTR: 32039.14.0256-307X.42.6.060601

1. Introduction. Floquet theory provides an ideal bridge between equilibrium and non-equilibrium quantum systems. Under periodic modulation with driving frequency $\omega_{\rm s} = 2\pi/T_{\rm s}$, the time evolution can be well described by a time-independent effective Hamiltonian.[1–3] Consequently, the scope of controlling and manipulating the quantum system is widely extended, and this so-called "Floquet engineering" becomes a conventional tool for tailoring exotic Hamiltonians.[4] A typical example is the Rabi model, which describes the interplay between light and matter and is strongly related to various important platforms of quantum sensing and quantum control,[5,6] such as nitrogen-vacancy (NV) centers,[7,8] trapped ions,[9,10] and optical lattice clocks.[11] If the frequency of the light $\omega_{\rm p}(t)$ is periodically modulated, the Hamiltonian within the rotating-wave-approximation (RWA) can be written as

$$\hat{H} = \frac{\hbar}{2}\left\{\left[\omega_0 - \omega_{\rm p}(t)\right]\hat{\sigma}_z + g\hat{\sigma}_x\right\}, \tag{1}$$

where $\hat{\sigma}_{z(x)}$ is the Pauli matrix labeling the longitudinal (transversal) interaction of the two-level atom with transition frequency ω_0, and g is the Rabi frequency. The driving form is $\omega_{\rm p}(t) = \bar{\omega}_{\rm p} - A\omega_{\rm s}\cos(\omega_{\rm s}t + \phi)$, in which $\bar{\omega}_{\rm p}$ is the mean value, A is the driving amplitude, and ϕ is the initial phase. Then, the carrier peak will be split into several Floquet sidebands at the detuning $\delta \equiv \omega_0 - \bar{\omega}_{\rm p} = k\omega_{\rm s}$, $k \in \mathbb{Z}$.

The Rabi frequency g controls the strength of quantum fluctuations, enabling the broadening of band peaks. Analogous to wave–particle duality, a small g will result in a sharp peak or more localization in the frequency space, akin to a particle in real space. Drawing a parallel to multiple-slit diffraction, different Floquet sidebands correspond to different channels, and $\omega_{\rm s}$ is like the distance between slits. Borrowing such a physical picture, in the high-frequency region where $g \ll \omega_{\rm s}$, the large inter-sideband distance in frequency space allows each Floquet sideband to be taken as an independent one, which is known as the resolved sideband approximation (RSBA).[11–14] However, the region beyond the high-frequency domain remains obscure in both theoretical and experimental aspects.

In this Letter, we propose the Floquet channel interference hypothesis (FCIH) for the region where $g \lesssim \omega_{\rm s}$. Drawing on the spirit of Thomas Young's double-slit experiment, increasing g and decreasing $\omega_{\rm s}$ can be analogized to enhancing the wave property of the Floquet mode and narrowing the distance between "slits" in frequency space. Consequently, as shown in Fig. 1, the interference pattern should be observed, and additional Floquet sidebands

*Corresponding authors. Email: tauwaang@cqu.edu.cn; zhangxf@cqu.edu.cn
© 2025 Chinese Physical Society and IOP Publishing Ltd. All rights, including for text and data mining, AI training, and similar technologies, are reserved.

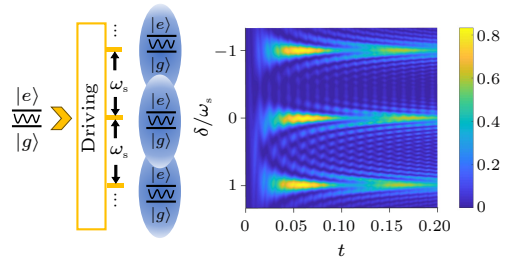

Fig. 1. The schematic diagrams of interference between Floquet modes in the frequency space. The interference pattern on the right side shows the numerical results of the excited population as a function of time t (s), the so-called Rabi spectrum, with $g/2\pi = 20.32\,\mathrm{Hz}$ and $\phi = 0$.

can emerge between integer ones, which we term non-integer Floquet sidebands (NIFBs). To demonstrate this, we design an experiment on a ^{87}Sr optical lattice clock platform. The experimental Rabi spectrum quantitatively agrees well with FCIH. The NIFBs can be significantly enhanced by the interference, and their height can be even comparable to the integer ones in Ramsey spectroscopy. Finally, the relationship between the initial phase and NIFBs is experimentally verified.

2. Methods. In the experiment, after a two-stage Doppler cooling process, about 10^4 ^{87}Sr atoms are cooled down to $\approx 3\,\mu\mathrm{K}$ and trapped in a one-dimensional optical lattice.[11,12,15] The lattice laser is set to the "magic wavelength" so that the AC Stark shifts of both the ground state ($^1\mathrm{S}_0$) and the excited state ($^3\mathrm{P}_0$) are the same. The long lifetime of the excited state ensures that spontaneous emission can be ignored.[14] The depth of the lattice potential is $V_0/E_\mathrm{r} \approx 93$ (where $E_\mathrm{r} = 3.44\,\mathrm{kHz}$ is the recoil energy), so that the tunneling between nearest neighbor sites is strongly suppressed and each site can be considered irrelevant to the others. All the atoms are initially prepared in the ground state. Then, the clock laser is added to excite atoms from the ground state to the excited state. At the same time, its frequency is periodically modulated as $\omega_\mathrm{p}(t)$ with $\omega_\mathrm{s}/2\pi = 100\,\mathrm{Hz}$. The misaligned angle between the lattice and the clock laser is $\delta\theta = 0.008$. Meanwhile, the longitudinal and transverse trap frequencies are $\nu_z = 64\,\mathrm{kHz}$ and $\nu_r = 250\,\mathrm{Hz}$, respectively.[12,16] For the Rabi spectroscopy, the probing time is set to $3T_\mathrm{s}$. On the other hand, in Ramsey spectroscopy, the dark time is $t_\mathrm{d} = 6T_\mathrm{s}$ and the probing time is $t_\mathrm{p} = 3T_\mathrm{s}$. Notice that, in order to avoid introducing additional discontinuity of the periodic driving, the clock laser is blocked during the dark time. Following our previous work,[12,14,16,17] the numerical results can be calculated with the help of the Runge–Kutta method. Considering thermal effects, we adopted the Boltzmann distribution; thus, the excited state population is[12]

$$\begin{aligned} P'_\mathrm{e}(\delta,t) &= \sum_{\boldsymbol{n}} q_z(n_z) q_r(n_r) P_\mathrm{e}(g_{\boldsymbol{n}})\,, \\ q_{z,r}(n_{z,r}) &= \frac{\mathrm{e}^{-\frac{h\nu_{z,r}}{k_\mathrm{B}T_{z,r}}}}{Z_{z,r}}\,, \quad Z_{z,r} = \sum_{z,r} \mathrm{e}^{-\frac{h\nu_{z,r}}{k_\mathrm{B}T_{z,r}}}\,, \end{aligned} \tag{2}$$

where δ is $\omega_0 - \omega_\mathrm{p}$, $q_z(n_z)$ and $q_r(n_r)$ are the statistical distributions of the atoms among eigenenergies of the harmonic oscillator approximated lattice trapping potential, $g_{\boldsymbol{n}} = g_0 \mathrm{e}^{-(\eta_z^2+\eta_r^2)/2} L_{n_r}(\eta_r^2) L_{n_z}(\eta_z^2)$ is the coupling strength for energy level $\boldsymbol{n}$, where L_n is the nth order Laguerre polynomial, and η is the Lamb–Dick parameters. The results quantitatively match very well with the experimental results in the deep optical lattice potential.

According to the Floquet sideband approximation (FSBA), the kth Floquet sideband can be understood as follows: the atom can be excited by absorbing the photon of the clock laser with the assistance of the kth Floquet photons. As a consequence, the Rabi frequency is renormalized as $g_k = gJ_{-k}[A]\mathrm{e}^{-\mathrm{i}k\phi}$ where $J_k[]$ is the kth order Bessel function of the first kind, A is the driving amplitude,[12] and the wave function contains an additional phase $\exp(-\mathrm{i}k\omega_\mathrm{s}t/2)$ that does not affect the excited population. However, the emergence of the NIFBs hints at strong interference effects beyond FSBA, so we propose the FCIH as follows:

> The quantum dynamics of the two-level atom at small g/ω_s is approximately determined by the interference of all Floquet channels.

3. Rabi Spectroscopy. Based on the FCIH, the excited population $P_\mathrm{e}(t)$ is determined by the interference of all the Floquet channels with effective detuning $\delta_k = \delta - k\omega_\mathrm{s}$, so it can be explicitly expressed as

$$\begin{aligned} P_\mathrm{e}(t) &= \left| \sum_k \Psi_k(t) \right|^2\,, \\ \Psi_k(t) &= -\frac{\mathrm{i}g_k}{\Omega_k} \sin\left(\frac{\Omega_k t}{2}\right) \mathrm{e}^{\frac{-\mathrm{i}k\omega_\mathrm{s}t}{2}}\,, \end{aligned} \tag{3}$$

where $\Omega_k = \sqrt{|g_k|^2 + \delta_k^2}$ [see Supplementary Materials (SM) for details]. Here, we want to emphasize that Eq. (3) can not be derived by the perturbation theory which we have already tried.

Under stroboscopic measurement $t = nT_\mathrm{s}$, phase Ψ_k depends only on g_k. Considering $g_k \to g_k^*$ under the transformation $\phi \to -\phi$, Ψ_k will change into $-\Psi_k^*$; accordingly, the excited population $P_\mathrm{e}(t)$ will not change based on FCIH. Therefore, the Rabi spectrum remains unchanged under the transformation $\phi \leftrightarrow -\phi$. Furthermore, if we implement the transformation $\phi \to \pi - \phi$, g_k is accordingly changed into g_{-k}, because of the Bessel function's property $J_{-k} = (-1)^k J_k$. Then, the excitation population $P_\mathrm{e}(t,\delta)$ will be transformed to $P_\mathrm{e}(t,-\delta)$. Therefore, we can find another symmetry $\{\delta \leftrightarrow -\delta, \phi \leftrightarrow \pi - \phi\}$. The analysis of the symmetries above is also suitable for the Ramsey spectrum.

The main contribution to the NIFB comes from the nearest-neighbor Floquet channels. To simplify the problem, we focus on the NIFB between $k = 0$ and $k = +1(-1)$ Floquet sidebands and name it the positive (negative) NIFB. Meanwhile, the driving amplitude in the experiment is adjusted to $A = 1.47$, satisfying $J_0[A] \approx J_1[A]$, so that the peak of the positive (negative) NIFB is located at $\delta = \omega_\mathrm{s}/2$, and the phase difference between the zero and first Floquet channels can be easily obtained as $\Delta\phi = \frac{\omega_\mathrm{s}t}{2} + \phi$. Neglecting the influences of other Floquet channels, the excited population P_e of positive and negative NIFBs under the stroboscopic measurement should

be approximately proportional to $\cos^2(\frac{\phi}{2})$ and $\sin^2(\frac{\phi}{2})$, respectively. Then, their difference follows $\cos(\phi)$ while tuning the initial phase ϕ.

The experimental results of the Rabi spectrum with different initial phases are presented in Fig. 2. Although the numerical results do not perfectly match the experimental data, many interesting features discussed above can still be recognized. At $\phi = 0$ in Fig. 2(a), the high positive peak indicates strong constructive interference, and the disappearance of the negative one hints at destructive interference. Such strong interference effects can also be clearly observed at $\phi = \pi$ in Fig. 2(c) with the positive and negative NIFBs exchanged. When ϕ is tuned to other values, the NIFBs are obscured by the system's noise, so they can be hardly distinguishable, as shown in Figs. 2(b), 2(d), and 2(e). However, all Rabi spectra can still reflect the validity of both symmetries $\phi \leftrightarrow -\phi$ and $\{\delta \leftrightarrow -\delta, \phi \leftrightarrow \pi - \phi\}$. Furthermore, the surprisingly good coincidence between the analytic and numerical results supports the effectiveness of the FCIH (see SM for details).

The positive and negative NIFBs are obscured by the system noise, but their difference can partially mitigate the influence of the noise. Thus, we introduce the asymmetry contrast

$$\chi = \frac{3}{\omega_s} \int_{\omega_s/3}^{2\omega_s/3} [P_e(\delta) - P_e(-\delta)]\, \mathrm{d}\delta\,, \tag{4}$$

where the integration range from one trough ($\delta = \omega_s/3$) to another ($\delta = 2\omega_s/3$) can further weaken the noise's influence. As demonstrated in Fig. 2(f), the deviation between experimental and numerical results becomes much smaller except at small ϕ values. Even more strikingly, both of them match well with FCIH's prediction and follow the cosine function.

As the evolution time increases, due to the significant impact of decoherence and noise on our experimental platform, we are constrained to investigate the NIFBs through numerical and analytical methods. As shown in Fig. 1 at $\phi = 0$, the NIFBs emerge one by one as time goes on, resembling the interference pattern of two traveling waves. Based on the FCIH, the troughs can be approximately determined by the destructive interference of zeroth and first Floquet sidebands. In Fig. 3, the black lines show the integer periods of two Floquet channels: $t = \frac{n}{\Omega_0(\delta)}$ and $t = \frac{m}{\Omega_1(\delta)}$ $(n, m \in \mathbb{Z})$. Then, the crossing points of black lines correspond to the commensurate value $\frac{\Omega_1}{\Omega_0} = \frac{m}{n}$ and indicate the local minima. From the color lines in Fig. 3, we can find the NIFBs are very stable, with their number increasing by two after each period $\frac{1}{\Omega_0(\omega_s/2)}$. However, the number of NIFBs in the blue curve ($t = 0.15$) in Fig. 3 violates the prediction above; that is because of the merging of some NIFBs into the integer ones, as illustrated in Fig. 1. Furthermore, we can find the heights of some NIFBs are comparable to those of the integer Floquet sidebands. This prompts the interesting question of whether the heights of NIFBs can surpass the integer ones in the experiment.

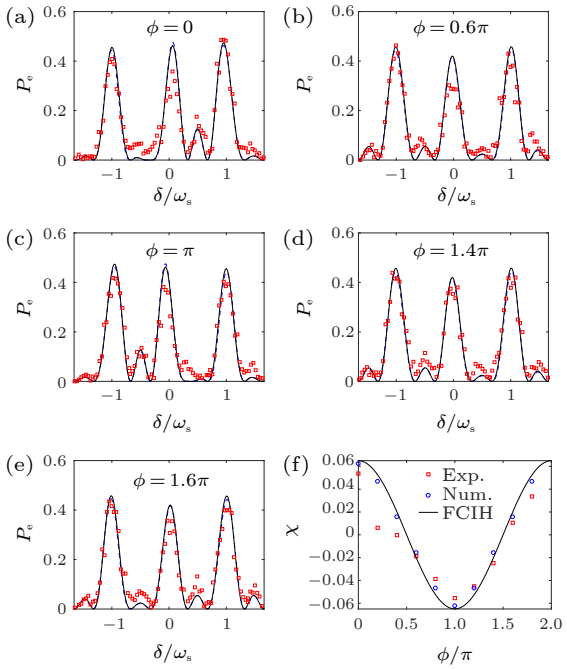

Fig. 2. (a)–(e) The experimental (red dots), numerical (black solid lines), and FCIH (blue dashed lines) results of the Rabi spectrum for different initial phases at $g/2\pi = 20.32\,\mathrm{Hz}$. (f) The asymmetry contrast parameter of the NIFBs for different initial phases.

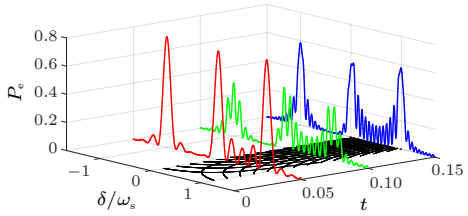

Fig. 3. The numerical results of the Rabi spectrum at $g/2\pi = 20.32\,\mathrm{Hz}$, $\phi = 0$, and $t = (0.05, 0.1, 0.15)$ (red, green, blue lines). The black lines indicate the integer multiples of periods for Ω_0 and Ω_1.

4. Ramsey Spectroscopy. To enhance the quality of the spectrum, it is straightforward to consider Ramsey's method, which involves the insertion of a freely evolving period between two probing pulses.[18] The excited population P_e can also be analytically obtained using the FCIH [see Supplemental Material (SM) for a discussion of further details about the FCIH and the robustness of NIFBs]. Differently, the kth Floquet wavefunction is expressed as

$$\Psi_k(t) = -\frac{2\mathrm{i}g_k}{\Omega_k} \mathrm{e}^{-\mathrm{i}\frac{k\omega_s(2t_p+t_d)}{2}} \sin\frac{\Omega_k t_p}{2} \left(\cos\frac{\Omega_k t_p}{2} \cos\frac{\delta_k t_d}{2} - \frac{\delta_k}{\Omega_k} \sin\frac{\Omega_k t_p}{2} \sin\frac{\delta_k t_d}{2} \right), \tag{5}$$

in which the phase only depends on g_k while employing the stroboscopic measurement. Therefore, same as the Rabi spectroscopy, the symmetries $\phi \to -\phi$ and $\{\delta \leftrightarrow -\delta, \phi \leftrightarrow \pi - \phi\}$ still hold.

The key idea of Ramsey spectroscopy is utilizing the interference to split the wide peak into several narrow ones,

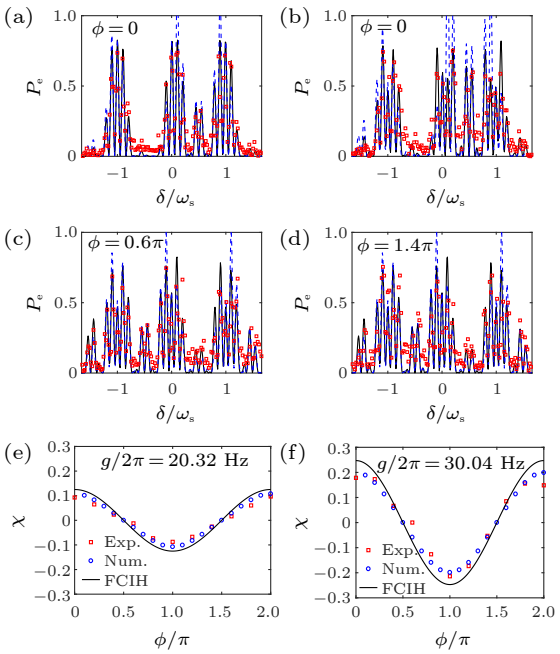

Fig. 4. The experimental (red dots), numerical (black solid lines), and FCIH (blue dashed lines) results of the Ramsey spectrum for different initial phases at (a) $g/2\pi = 20.32\,\mathrm{Hz}$ and (b)–(d) $g/2\pi = 30.04\,\mathrm{Hz}$. (e) and (f) The asymmetry contrast of the NIFBs for different initial phases.

with linewidths inversely proportional to t_d. In Figs. 4(a)–4(d), it becomes apparent that all the integer Floquet sidebands split into numerous narrow peaks. Notably, the Ramsey NIFBs with multiple peaks also emerge. These peaks exhibit high sensitivity to the initial phases and satisfy both symmetries, too.

As illustrated in Fig. 4(a), the numerical and FCIH results match well with the experimental data, particularly concerning the NIFBs. In comparison to the Rabi spectroscopy, the height of the Ramsey NIFBs is much larger ($P_\mathrm{e} = 0.32$). After that, we increase the probe laser power and adjust the Rabi frequency to $g/2\pi = 30.04\,\mathrm{Hz}$. As shown in Figs. 4(b)–4(d), the intensity of the NIFBs is notably amplified, and the symmetries still hold. In the experiment, the maximum peak height of the NIFB can reach 0.6 [see Fig. 4(b)], and the numerical simulation suggests that it could exceed 0.9 with a further increase in g. However, immediate verification is impeded by the constraints of our experimental platform.

Indeed, despite the frequency interval of only 2 Hz in our experiment, ensuring the distinctiveness of each Ramsey peak remains a challenge. At large g, the numerical and experimental results still exhibit good agreement, whereas the FCIH results can only offer qualitative insights due to normalization issues. However, through integration, the asymmetry contrast χ significantly enhances the accuracy. As demonstrated in Figs. 4(e) and 4(f), both numerical and experimental results achieve a very good agreement with the FICH's prediction: following the cosine function.

5. Conclusion and Discussion. Floquet sideband spectroscopy beyond RSBA is systematically investigated using both experimental and numerical methods. The proposed FCIH offers a quantitative description of the interference between different Floquet channels at small g/ω_s. Building upon FCIH, we have identified two distinct symmetries associated with the initial phase, which have been validated through Rabi and Ramsey spectroscopies. As the value of g/ω_s increases, the peaks of NIFBs grow significantly, even reaching a magnitude comparable to that of the integer Floquet sidebands. Additionally, we have introduced a new parameter called asymmetry contrast χ, which serves to mitigate the impact of noise and reflects the dependence on the initial phase. Furthermore, we have discussed the influence of spontaneous emission from the excited state and noise in SM.

Our theoretical analysis is not limited to optical lattice clocks; it can also be immediately applied to other platforms, such as NV-center,[19–21] superconducting qubit,[22] or trapped ions.[9,10,23,24] In these systems, relatively moderate coherent time may limit the visibility of the interference, but the general properties of NIFBs are robust under the influence of noise and decoherence,[25] as shown in the section II of SM. Although the interference phenomena of Floquet modes discussed in our work pertain to single-body systems, we believe that their implications may also extend to quantum many-body systems.

Acknowledgements. This work was supported by the National Natural Science Foundation of China (Grant No. 12274045). X.-F. Z. acknowledges support from the National Natural Science Foundation of China (Grant Nos. 12274046, 11874094, 12147102, and 12347101), the Natural Science Foundation of Chongqing (Grant No. CSTB2022NSCQ-JQX0018), the Fundamental Research Funds for the Central Universities (Grant No. 2021CDJZYJH-003), and the Xiaomi Foundation/Xiaomi Young Talents Program.

References

[1] Eckardt A and Holthaus M 2007 *EPL* **80** 50004
[2] Vogl M, Laurell P, Barr A D, and Fiete G A 2019 *Phys. Rev. X* **9** 021037
[3] Bukov M, D'Alessio L and Polkovnikov A 2015 *Adv. Phys.* **64** 139
[4] Eckardt A 2017 *Rev. Mod. Phys.* **89** 011004
[5] Zeng J, Yang C H, Dzurak A S, and Barnes E 2019 *Phys. Rev. A* **99** 052321
[6] Cai M L, Liu Z D, Zhao W D, Wu Y K, Mei Q X, Jiang Y, He L, Zhang X, Zhou Z C, and Duan L M 2021 *Nat. Commun.* **12** 1126
[7] Dobrovitski V V, Fuchs G D, Falk A L, Santori C, and Awschalom D D 2013 *Annu. Rev. Condens. Matter Phys.* **4** 23
[8] Golter D A, Oo T, Amezcua M, Stewart K A, and Wang H 2016 *Phys. Rev. Lett.* **116** 143602
[9] Wineland D J, Barrett M, Britton J, Chiaverini J, DeMarco B, Itano W M, Jelenkovic B, Langer C, Leibfried D, Meyer V, Rosenband T, and Schatz T 2003 *Philosophical Transactions of the Royal Society of London Series A* **361** 1349
[10] Blatt R and Roos C F 2012 *Nat. Phys.* **8** 277

[11] Blatt S, Thomsen J W, Campbell G K, Ludlow A D, Swallows M D, Martin M J, Boyd M M, and Ye J 2009 *Phys. Rev. A* **80** 052703
[12] Yin M J, Wang T, Lu X T, Li T, Wang Y B, Zhang X F, Li W D, Smerzi A, and Chang H 2021 *Chin. Phys. Lett.* **38** 073201
[13] Vogl M, Rodriguez-Vega M, and Fiete G A 2020 *Phys. Rev. B* **101** 024303
[14] Lu X T, Wang T, Li T, Zhou C H, Yin M J, Wang Y B, Zhang X F, and Chang H 2021 *Phys. Rev. Lett.* **127** 033601
[15] Wang Y B, Yin M J, Ren J, Xu Q F, Lu B Q, Han J X, Guo Y, and Chang H 2018 *Chin. Phys. B* **27** 023701
[16] Zhou Y H, Zhang X F, and Wang T 2023 *Phys. Rev. A* **108** 033304
[17] Yin M J, Lu X T, Li T, Xia J J, Wang T, Zhang X F, and Chang H 2022 *Phys. Rev. Lett.* **128** 073603
[18] Ramsey N F 1950 *Phys. Rev.* **78** 695
[19] Cui J M, Chen X D, Fan L L, Gong Z J, Zou C W, Sun F W, Han Z F, and Guo G C 2012 *Chin. Phys. Lett.* **29** 036103
[20] Schirhagl R, Chang K, Loretz M, and Degen C L 2014 *Annu. Rev. Phys. Chem.* **65** 83
[21] Acosta V and Hemmer P 2013 *MRS Bulletin* **38** 127
[22] Ye Y, Cao S, Wu Y *et al.* 2021 *Chin. Phys. Lett.* **38** 100301
[23] Leibfried D, Blatt R, Monroe C, and Wineland D 2003 *Rev. Mod. Phys.* **75** 281
[24] Zhang Q, Wang Y, Zhu C, Wang Y, Zhang X, Gao K, and Zhang W 2020 *Chin. Phys. B* **29** 093203
[25] Manzano D 2020 *AIP Advances* **10** 025106